Quasielastic neutron scattering study of hydrogen motion in C15-type TaV_2H_x

1998 J. Phys.: Condens. Matter 10 1787

(http://iopscience.iop.org/0953-8984/10/8/012)

J. Phys.: Condens. Matter **10** (1998) 1787–1801. Printed in the UK PII: S0953-8984(98)87599-1

Quasielastic neutron scattering study of hydrogen motion in C15-type TaV_2H_x

A V Skripov†, J C Cook‡‖, D S Sibirtsev†, C Karmonik§‖ and R Hempelmann§

† Institute of Metal Physics, Urals Branch of the Academy of Sciences, Ekaterinburg 620219, Russia

‡ Institut Laue–Langevin, F-38042 Grenoble, France

§ Institut für Physikalische Chemie, Universität des Saarlandes, D-66041 Saarbrücken, Germany

Received 15 September 1997, in final form 5 December 1997

Abstract. In order to clarify the mechanism of hydrogen diffusion in cubic Laves phase TaV_2, we have performed high-resolution quasielastic neutron scattering measurements on TaV_2H_x ($x = 0.6$ and 1.1) in the temperature range 10–320 K. It is found that the diffusive motion of hydrogen in this system can be described in terms of two jump processes: the fast localized H motion within hexagons formed by interstitial g (Ta_2V_2) sites and the slower hopping from one hexagon to the other. This model is also supported by neutron diffraction measurements showing that the sublattice of g sites in TaV_2D_x is split into hexagons well separated from each other. The behaviour of the elastic incoherent structure factor for TaV_2H_x suggests that only a fraction of the H atoms participate in the fast localized motion, and this fraction increases with temperature. Comparison of the properties of TaV_2H_x and other Laves phase hydrides with g-site occupation shows a clear correlation between the parameters of the two jump processes and the g–g distances r_1 (within the hexagons) and r_2 (between different hexagons).

1. Introduction

Nuclear magnetic resonance (NMR) measurements of ^{1}H, ^{2}D and ^{51}V spin–lattice relaxation rates in the cubic Laves phase hydrides TaV_2H_x (TaV_2D_x) [1, 2] have revealed a coexistence of two types of hydrogen hopping with different frequency scales. At $T \leqslant 200$ K the two frequency scales differ by several orders of magnitude. The faster motion is identified as a localized hydrogen hopping. This localized motion appears to be intrinsic (i.e., not related to hydrogen trapped by impurities or defects). It is not frozen out on the frequency scale 10^7–10^9 s^{-1} down to 30 K. The main features of the fast localized H (D) motion found from the NMR experiments [1, 2] are as follows. (1) The temperature dependence of the hopping rate τ_1^{-1} is non-Arrhenius. (2) The hopping rate strongly depends on hydrogen concentration, decreasing with increasing H (D) content. (3) There is a pronounced effect of isotope (H $\leftrightarrow$ D) substitution on the parameters of the localized motion. However, the geometrical aspects of hydrogen motion could not be determined from NMR experiments. The aim of the present work is to clarify the microscopic picture of H hopping in TaV_2H_x using incoherent quasielastic neutron scattering (QENS) measurements which are sensitive both to the spatial and frequency scales of atomic motion.

‖ Present address: National Institute of Standards and Technology, Gaithersburg, MD 20899, USA.

0953-8984/98/081787+15$19.50

The cubic C15-type intermetallic compound TaV_2 can absorb considerable amounts of hydrogen, forming homogeneous solid solutions TaV_2H_x ($x \leqslant 1.7$) [3]. According to the neutron diffraction data [4–6], D atoms in TaV_2D_x occupy only tetrahedral sites of g type (Ta_2V_2), the other two types of tetrahedral sites, e (TaV_3) and b (V_4), being empty. For all x, the single-phase state of TaV_2H_x (TaV_2D_x) with the C15 host-lattice structure is retained down to 4 K. In compounds with $x \geqslant 1.3$ the ordering of H (D) is observed below 150 K [6]. This ordering may be related to the unusual H (D) dynamics in TaV_2H_x (TaV_2D_x). Such a relation has been found, for example, for α-YH_x and α-ScH_x [7] where both the anomalous H motion and the pronounced short-range order (pairing) are observed.

In this work we report the results of our high-resolution QENS measurements for TaV_2H_x ($x = 0.6$ and 1.1) for the temperature range 10–320 K. Some preliminary results for $TaV_2H_{0.6}$ have been published in our previous letter [8]. The emphasis is placed on the study of the fast localized H motion. Analysis of the experimental QENS spectra supported by the neutron diffraction results has enabled us to elucidate the microscopic picture of H hopping in TaV_2H_x. We also discuss the systematics of H motion in cubic Laves phase hydrides with g-site occupation and show, in particular, why the fast localized motion is most pronounced in TaV_2H_x.

2. Experimental details

The preparation of TaV_2H_x samples was analogous to that described in [1]. X-ray diffraction analysis has shown that both $TaV_2H_{0.6}$ and $TaV_2H_{1.1}$ are single-phase solid solutions with the C15-type host-lattice structure and the lattice parameters $a_0 = 7.22$ and 7.27 Å, respectively.

Table 1. Experimental parameters for QENS measurements on TaV_2H_x.

Sample	Spectrometer	λ_i (Å)	T-range (K)	$\hbar\omega$-range (meV)	Resolution (μeV)	Q-range (Å^{-1})
$TaV_2H_{0.6}$	IN10, Si(111)	6.271	10–140	−0.0135–+0.0135	1.0	0.41–1.94
	IN5	5.0	10, 220–300	−100–+2.42	109	0.09–2.18
$TaV_2H_{1.1}$	IN10, Si(111)	6.271	10–160, 320	−0.0135–+0.0135	1.0	0.41–1.94
	IN10, Si(311)	3.275	10, 140–160	−0.0235–+0.0235	3.5	1.77–3.69
	IN5	5.0	10, 200–300	−235–+2.37	109	0.33–2.18

QENS measurements were performed on the high-resolution backscattering spectrometer IN10 and the cold-neutron time-of-flight spectrometer IN5 at the Institut Laue–Langevin (ILL) in Grenoble. These two spectrometers complement each other with respect to the resolution and the accessible range of energy transfer $\hbar\omega$, providing one with the opportunity to probe hydrogen motion in the range of hopping rates 10^8–10^{11} s^{-1}. In order to extend the range of momentum transfer $\hbar Q$, in addition to the standard IN10 configuration with a Si(111) monochromator and analysers, we have also used the set-up with a Si(311) monochromator and analysers ($Q_{max} \approx 3.7$ Å^{-1}). The experimental conditions including the temperature ranges, the incident neutron wavelengths λ_i, the energy resolution (FWHM) and the ranges of $\hbar\omega$ and Q are listed in table 1.

The powdered TaV_2H_x samples were placed into flat Al containers with a depth of 1.1 mm. In the experiments on IN10 with Si(111) analysers the plane of the container was oriented in the direction of the only Bragg reflection ($2\theta \approx 98^\circ$) in the Q-range studied. The same orientation of the container plane was used in the course of the measurements on IN10 with Si(311) analysers; in this case a considerable fraction of the analyser plate surfaces

had to be shielded by cadmium in order to avoid Bragg reflections from the sample, the container and the cryostat. In the experiments on IN5 the plane of the container was parallel to the line $2\theta = 135^\circ$ (the highest-angle limit of the detector bank). The raw experimental data were corrected for absorption and self-shielding using the standard ILL programs.

For both spectrometers the instrumental resolution functions were determined from the measured QENS spectra of TaV_2H_x at 10 K. The background spectra were measured for identical outgassed TaV_2 samples at 140 K (IN10) and 220 K (IN5) in the same experimental geometry as for TaV_2H_x. The scattering function $S_{\mathrm{exp}}(Q, \omega)$ of the hydrogen sublattice was determined by subtracting these background spectra from the TaV_2H_x spectra.

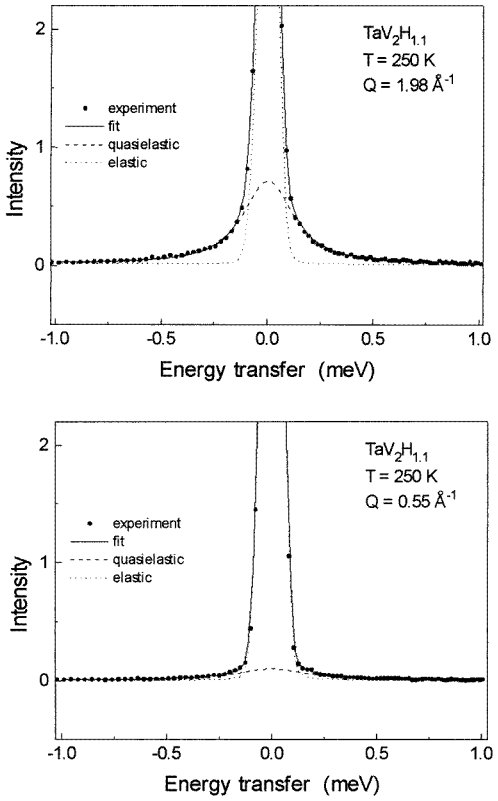

Figure 1. Quasielastic neutron scattering spectra for $TaV_2H_{1.1}$ measured on IN5 at 250 K and two Q-values (0.55 and 1.98 $\mathrm{Å}^{-1}$). The solid lines show the results of the fits of the two-component model to the data. The dotted lines represent the spectrometer resolution function ('elastic' component) and the dashed lines show the Lorentzian 'quasielastic' component.

3. Results and discussion

3.1. QENS spectra

Most of the experimental QENS spectra can be satisfactorily described by a sum of two components: a narrow 'elastic' line represented by the spectrometer resolution function $R(Q, \omega)$ and a resolution-broadened Lorentzian 'quasielastic' line. As an example of the data, figure 1 shows two spectra of $TaV_2H_{1.1}$ recorded at 250 K for different Q-values. As

the first step of the analysis, we have fitted $S_{\mathrm{exp}}(Q, \omega)$ with the model incoherent scattering function

$$S_{\mathrm{inc}}(Q, \omega) = A_0(Q)\delta(\omega) + [1 - A_0(Q)]L(\omega, \Gamma) \tag{1}$$

convoluted with $R(Q, \omega)$. Here $\delta(\omega)$ is the 'elastic' δ-function, $L(\omega, \Gamma)$ is the 'quasielastic' Lorentzian with the half-width Γ and $A_0(Q)$ is the elastic incoherent structure factor (EISF). The 'quasielastic' component has not been detected below 75 K for $TaV_2H_{0.6}$ and below 105 K for $TaV_2H_{1.1}$. At higher temperatures the relative intensity of this component is found to increase with increasing Q, its half-width Γ being nearly Q-independent. These features are typical of the case of spatially confined (localized) motion [9]. The value of Γ is proportional to the hydrogen hopping rate τ_1^{-1}, and $A_0(Q)$ contains information on the geometry of the localized motion [9].

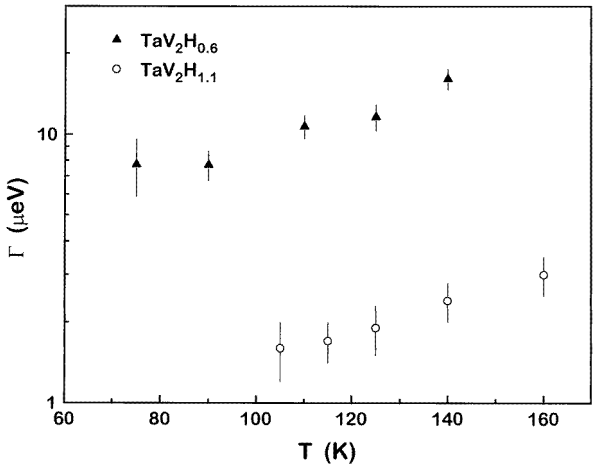

Figure 2. The temperature dependence of the half-width (HWHM) of the 'quasielastic' line for $TaV_2H_{0.6}$ and $TaV_2H_{1.1}$, as measured on IN10.

In order to assess Γ and $A_0(Q)$ at each temperature, we have used a simultaneous fit of $S_{\mathrm{inc}}(Q, \omega)$ to the data at all Q with a common value of Γ. The temperature dependence of the fitted quasielastic half-width Γ resulting from the measurements on IN10 and IN5 is shown in figures 2 and 3, respectively. It can be seen that the value of Γ increases with increasing temperature and decreases with increasing hydrogen content. This qualitatively agrees with the NMR results [1, 2] indicating the strong decrease in the hopping rate τ_1^{-1} with increasing H concentration. Figure 4 shows the behaviour of the elastic incoherent structure factor $A_0(Q)$ for $TaV_2H_{1.1}$ at four temperatures. Similar behaviour of $A_0(Q)$ is observed for $TaV_2H_{0.6}$. The measured EISF shows pronounced temperature dependence, decreasing with increasing T. In order to account for this feature, we have to assume that only a fraction p of H atoms participates in the fast localized motion, and this fraction increases with temperature. The fraction $1 - p$ of 'static' protons (on the frequency scale determined by the spectrometer resolution) contributes only to the 'elastic' line and makes the observed values of $A_0(Q)$ higher than those expected in the case of $p = 1$.

The temperature-dependent fraction of H atoms participating in the fast localized motion has been also reported for α-ScH_x [7]. The existence of 'static' protons is expected to originate from the H–H interaction leading to the formation of some ordered atomic configurations at low temperatures. In fact, neutron diffraction measurements [6] have

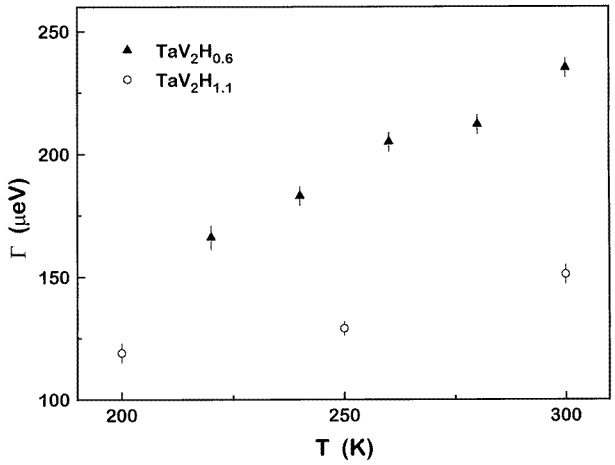

Figure 3. The temperature dependence of the half-width (HWHM) of the 'quasielastic' line for $TaV_2H_{0.6}$ and $TaV_2H_{1.1}$, as measured on IN5.

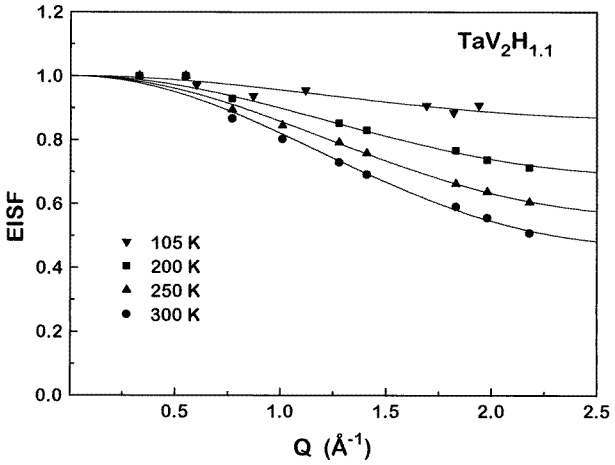

Figure 4. The elastic incoherent structure factor for $TaV_2H_{1.1}$ as a function of Q at $T = 105$, 200, 250 and 300 K. The solid lines represent the fits of the six-site model (equation (3)) with the fixed $r = 0.99$ Å to the data.

revealed the long-range ordering of D in TaV_2D_x with $x \geqslant 1.3$. For lower hydrogen concentrations a short-range order is likely to exist. Because of the thermal activation, the ordered H configurations tend to disappear at high temperatures; this results in the observed growth of the fraction p with increasing T.

3.2. The geometry of the localized H motion

In order to elucidate the geometry of the localized H motion, we have to analyse the behaviour of EISF as a function of Q. As has been shown previously [8], the experimental results are not consistent with the model of H hopping between two closely spaced sites. Furthermore, the structure of the network of interstitial sites for the C15 lattice does not

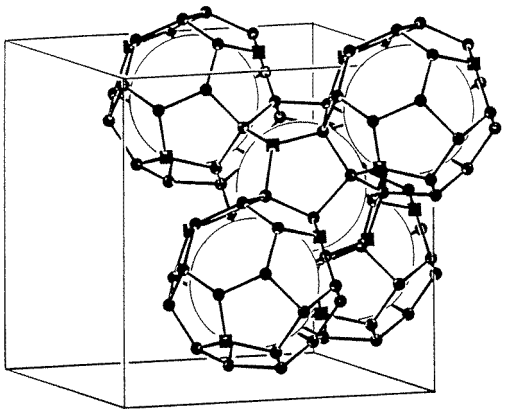

Figure 5. The spatial arrangement of interstitial sites in C15-type AB_2 compound (from [10]). Full squares: e sites; full circles: g sites; large open circles: A atoms.

suggest the existence of pairs well separated from the other sites. The spatial arrangement of g and e sites is shown schematically in figure 5. Each g site has four nearest neighbours: two g sites at a distance $r_1 \approx 0.153a_0$, one g site at $r_2 \approx 0.175a_0$ and one e site at $r_3 \approx 0.153a_0$. For the value $a_0 = 7.27$ Å corresponding to $TaV_2H_{1.1}$ these distances are equal to 1.11, 1.27 and 1.11 Å, respectively. Note that these distances are calculated for the 'ideal' positional parameters of g and e sites in the C15 structure, as derived from the conditions of the closest packing of hard spheres. The actual positions of H atoms in C15-type intermetallics may be displaced from the 'ideal' ones (see below).

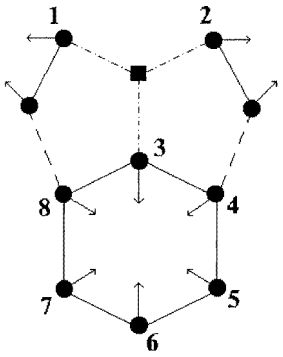

Figure 6. A schematic representation of a part of the network of interstitial g sites (circles) and e sites. Solid, dashed and chain lines represent the distances r_1, r_2 and r_3, respectively. Models (i) and (ii) correspond to jumps between sites 1–2–3 and 3–4–5–6–7–8, respectively. The arrows show the directions of displacements of the hydrogen atoms in TaV_2 from their 'ideal' positions in the tetrahedra.

Taking into account that H atoms occupy only g sites [4–6], we may conclude that there are two models of the localized H motion consistent with the structure of the network of g sites. These two models are illustrated by figure 6.

(i) Hopping between three sites on a circle of radius $r \approx r_3$. This model corresponds to H jumps between three g sites that are the nearest neighbours of one e site (see figure 6).

Although the model implies H jumps to third-neighbour g sites, one may expect that if the potential barriers for g–g jumps via intermediate e sites are lower than for the nearest-neighbour g–g jumps, the motion of a hydrogen atom will be confined to the first coordination sphere of the e site. In this case the form of the EISF allowing for the temperature-dependent p is

$$A_0(Q,T) = 1 - p(T) + \frac{1}{3}p(T)[1 + 2J_0(Qr\sqrt{3})] \tag{2}$$

where $J_0(x)$ is the Bessel function of zeroth order.

(ii) Hopping between six sites on a circle of radius $r \approx r_1$. This model corresponds to H jumps between six g sites forming hexagons in $\langle 111 \rangle$ directions (see figures 5 and 6). Since the distance between the nearest g sites within the hexagon (r_1) is shorter than the distance between the nearest g sites on different hexagons (r_2), the motion of a hydrogen atom may be confined to one hexagon. For this model

$$A_0(Q,T) = 1 - p(T) + \frac{1}{6}p(T)[1 + 2J_0(Qr) + 2J_0(Qr\sqrt{3}) + J_0(2Qr)]. \tag{3}$$

If the values of radius r in equations (2) and (3) are nearly the same, i.e. $r_3 \approx r_1$, the Q-dependence of A_0 for model (ii) nearly coincides with that for model (i) in the range $Qr \leqslant 2$ (see, for example, figure 6.13 of reference [9]). Therefore it would be impossible to distinguish between models (i) and (ii) from the Q dependence of A_0 up to $Q_{\max} \approx 2$ Å^{-1}, i.e. in the experimental range of our measurements on IN5 and IN10 with Si(111).

We now consider the actual structure of the hydrogen sublattice resulting from the neutron diffraction measurements for TaV_2D_x [4–6]. These measurements have revealed considerable displacements of D atoms from the 'ideal' positions in the tetrahedra. The directions of the displacements are shown by arrows in figure 6. The pattern of these displacements is such that the shorter g–g distances (r_1) become shorter, whereas the longer ones (r_2) become longer. Using the experimental positional parameters of hydrogen atoms at g sites ($X = 0.055$, $Z = 0.888$) [6] to calculate g–g distances in $TaV_2H_{1.1}$, we obtain $r_1 = 0.99$ Å, $r_2 = 1.44$ Å. The r_2/r_1 ratio is equal to 1.45; this value should be compared with the 'ideal' one, $1.27/1.11 = 1.14$. This means that the sublattice of g sites in TaV_2H_x is split into hexagons *well separated from each other*. Therefore a hydrogen atom may perform many jumps within a hexagon before jumping to the other hexagon. Thus, the actual structure of the hydrogen sublattice supports the six-site model (ii).

Let us check now whether this model is consistent with the observed Q-dependence of A_0. The fit of equation (3) to the $TaV_2H_{1.1}$ data at 300 K (corresponding to the widest range of $A_0(Q)$ variation) with p and r as free parameters yields $p = 0.60 \pm 0.05$, $r = 1.02 \pm 0.09$ Å. The fitted value of r agrees with the value $r_1 = 0.99$ Å resulting from the structure. Similar fitting of the three-site model (equation (2)) to the $TaV_2H_{1.1}$ data at 300 K yields $p = 0.62 \pm 0.05$, $r = 0.99 \pm 0.08$ Å. However, in this case the fitted r-value should be compared with the radius $r_3 = 1.15$ Å determined for $TaV_2H_{1.1}$ using the actual positional parameters. Thus, for the three-site model the radius of H motion obtained from the best fit of $A_0(Q)$ does not coincide with the corresponding radius determined by the structure. By fixing the value of r to 0.99 Å, we have found reasonable fits of the six-site model (equation (3)) to the data at all temperatures with p as the only fit parameter. The results of these fits are shown as solid lines in figure 4.

In order to extend the measurements to the region of higher Q, we have recorded QENS spectra of $TaV_2H_{1.1}$ at $T = 140$ and 160 K using the IN10 spectrometer with Si(311) analysers. Figure 7 shows the observed behaviour of EISF in the extended Q-range. It should be noted that at both temperatures the EISF is found to be nearly constant between

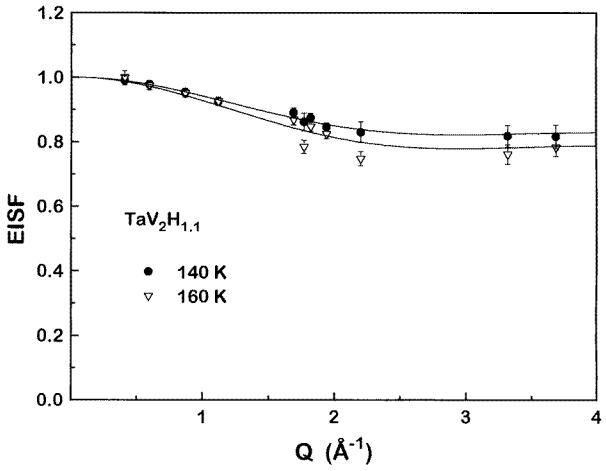

Figure 7. The elastic incoherent structure factor for $TaV_2H_{1.1}$ at 140 and 160 K as a function of Q. The solid lines show the fits of the six-site model (equation (3)) with the fixed $r = 0.99$ Å to the data.

2.2 and 3.7 Å^{-1}. The solid lines in figure 7 show fits of the six-site model (ii) with the fixed $r = 0.99$ Å to the data.

In order to obtain parameters of the localized H motion at each temperature, we have used a simultaneous fit of $S_{\mathrm{inc}}(Q, \omega)$ for the six-site model with the fixed $r = 0.99$ Å to the data at all Q. Taking into account that only a fraction p of protons participates in the fast localized motion, $S_{\mathrm{inc}}(Q, \omega)$ for the six-site model [9] can be written in the form

$$S_{\mathrm{inc}}(Q, \omega) = A_0(Q)\delta(\omega) + p\sum_{i=1}^{3} A_i(Q)L(\omega, \Gamma_i) \tag{4}$$

where $A_0(Q)$ is given by equation (3), $L(\omega, \Gamma_i)$ is the Lorentzian function with the half-width Γ_i, $\Gamma_1 = 0.5\tau_1^{-1}$, $\Gamma_2 = 1.5\tau_1^{-1}$, $\Gamma_3 = 2\tau_1^{-1}$ and τ_1 is the mean time between two successive jumps of a proton. Thus, for the six-site model the quasielastic line is expected to consist of three Lorentzian components with different half-widths Γ_i and Q-dependent amplitudes $A_i(Q)$, and the half-width of the composite quasielastic line should show a certain Q-dependence, especially at $Qr \geqslant 1.5$ [9]. However, as has been noted previously [11], because of the limited experimental accuracy it is difficult to distinguish between such a three-component quasielastic line and a single Lorentzian with a Q-independent width in the case of a rather weak quasielastic line coexisting with a strong elastic one. In fact, we have found that the quality of simultaneous fits based on equation (4) with the fit parameters τ_1^{-1} and p is comparable to the quality of simultaneous fits based on equations (1) and (3) with a common Γ. Moreover, the values of p obtained from these two types of fit are nearly the same, and the common Γ value appears to be close to $0.6\tau_1^{-1}$. This means that the observed shape of the quasielastic line is not always a good indicator of the type of localized motion. On the other hand, the Q-dependence of EISF is usually measured accurately enough to form a solid basis for an analysis of the geometry of localized motion.

Figure 8 shows the temperature dependence of p resulting from the fits of equation (4) to the data for $TaV_2H_{0.6}$ and $TaV_2H_{1.1}$. The usual approach to the description of $p(T)$ is based on the assumption of a certain energy gap ΔE between 'static' and 'mobile' H states

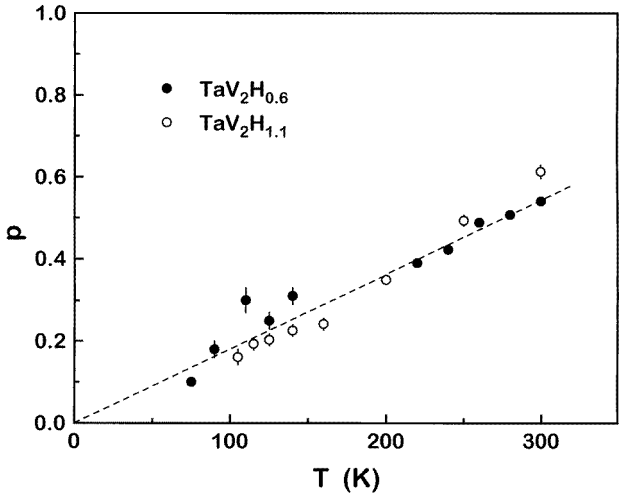

Figure 8. The temperature dependence of the fraction of protons participating in the fast localized motion, as determined from the fits of the six-site model to the data for $TaV_2H_{0.6}$ and $TaV_2H_{1.1}$. The dashed line shows a linear $p(T)$ fit for $TaV_2H_{0.6}$.

(see, e.g., [7]). In this case,

$$p(T) = \frac{b(T)}{1 + b(T)} \tag{5}$$

$$b(T) = b_{\mathrm{m}} \exp(-\Delta E / k_{\mathrm{B}} T) \tag{6}$$

where b_{m} is the relative degeneracy factor of 'mobile' states. We have found, however, that such a model can only describe the observed $p(T)$ if there is a broad ΔE distribution. In fact, as can be seen from figure 8, the observed $p(T)$ for $TaV_2H_{0.6}$ may be reasonably approximated by a linear dependence. This feature resembles the well-known behaviour of glasses originating from two-level systems with a nearly uniform ΔE distribution at low ΔE [12]. The existence of the ΔE distribution in TaV_2H_x may be ascribed to a spread in local H configurations, as is typical of non-stoichiometric hydrides. At low T the values of $p(T)$ decrease with increasing H content (see figure 8). This is consistent with the idea (discussed in section 3.1) that H–H interactions tend to suppress the fast localized motion. In particular, because of the 'blocking' effect [13] the localized H motion over a hexagon seems to be impossible if this hexagon is populated by more than one H atom. The average population of one H atom per g-site hexagon corresponds to the composition TaV_2H_2; for $TaV_2H_{0.6}$ and $TaV_2H_{1.1}$ the average population is 0.3 and 0.55 H atoms per hexagon, respectively.

3.3. Effects of the long-range diffusion

The NMR data [2] suggest that the hopping of H atoms between different hexagons may become observable on the IN10 frequency scale at $T \geqslant 300$ K. In order to verify this, we have measured QENS spectra of $TaV_2H_{1.1}$ at 320 K using IN10 with Si(111) analysers. At this temperature the hopping rate of the localized H motion is much higher than the frequency 'window' of IN10; therefore, instead of the low-temperature 'quasielastic' line we observe a flat background. As expected, this background is Q-dependent, increasing with increasing Q. On the other hand, the low-temperature 'elastic' line is now broadened

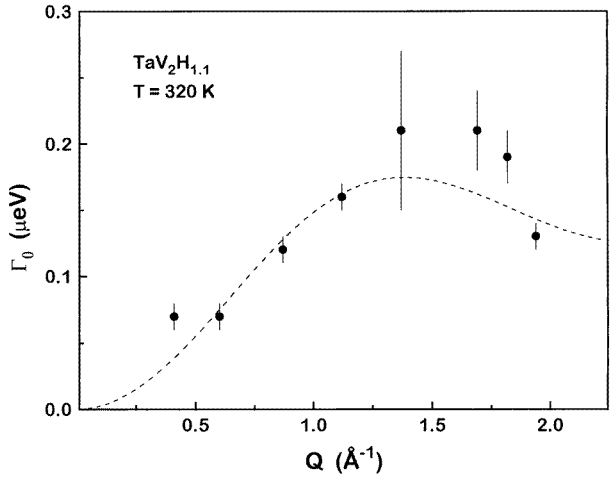

Figure 9. The half-width of the Lorentzian QENS component for $TaV_2H_{1.1}$ measured on IN10 at 320 K as a function of Q. The dashed line shows the fit of the Chudley–Elliott model (equation (7)) to the data.

due to H jumps from one hexagon to the other, i.e. due to H jumps leading to the long-range diffusion.

The observed QENS spectra at 320 K can be well described by a sum of a flat background and a single Lorentzian convoluted with the instrumental resolution function. The Q-dependence of the half-width Γ_0 of this Lorentzian is shown in figure 9. The observed shape of $\Gamma_0(Q)$ with the maximum is typical of the case of jump diffusion. For parametrization of this dependence we have used the orientationally averaged Chudley–Elliott model [14] describing the diffusion with the constant jump length l and with random distribution of jump directions. The corresponding form of $\Gamma_0(Q)$ is

$$\Gamma_0(Q) = \frac{6\hbar D}{l^2}\left(1 - \frac{\sin Ql}{Ql}\right) \tag{7}$$

where D is the tracer diffusion coefficient. The fit of equation (7) to the data is shown by the dashed line in figure 9; the values of the fit parameters are $D = (3.8 \pm 0.3) \times 10^{-8}$ cm^2 s^{-1}, $l = 3.25 \pm 0.12$ Å. These values should be considered only as rough estimates, since the Chudley–Elliott model is not strictly applicable to H diffusion in our system. Furthermore, at 320 K the observed broadening is still rather small. Nevertheless, the fitted value of D appears to be close to the value $D_{\mathrm{PFG}}(320\ \mathrm{K}) = (2.5 \pm 0.6) \times 10^{-8}$ cm^2 s^{-1} extrapolated from the pulsed-field-gradient NMR measurements of H diffusivity in $TaV_2H_{1.24}$ in the range 334–484 K [15]. On the other hand, the effective jump length l is considerably longer than the distance between the nearest g sites on different hexagons, $r_2 = 1.44$ Å. A similar feature has been reported for the other Laves phase hydrides, including $ZrV_2H_{2.9}$ [16], $HfV_2H_{3.3}$ [17] and $ZrCr_2H_x$ [18]. This feature can be naturally explained in terms of our model implying two frequency scales of H motion: the rate of hopping within a g-site hexagon (τ_{l}^{-1}) and the rate of hopping between hexagons (τ_{d}^{-1}) with $\tau_{\mathrm{d}}^{-1} \ll \tau_{\mathrm{l}}^{-1}$. In this model τ_{d} is the mean residence time of a hydrogen atom *at a hexagon*. Since a H atom may enter a hexagon through one site and leave it from the other site, the total displacement for the time τ_{d} is r_2 plus the additional displacement between the initial and the final positions of a hydrogen atom at the hexagon. Both the half-width Γ_0 and the main maximum of

the spin–lattice relaxation rate in NMR experiments [2, 19] are determined by the slower frequency scale τ_d^{-1}; therefore the apparent jump length l derived from these measurements is considerably longer than r_2.

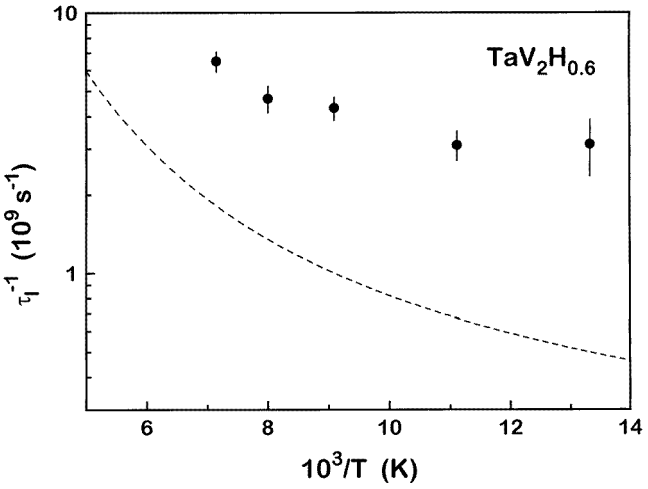

Figure 10. The temperature dependence of the hydrogen hopping rate τ_l^{-1} for $TaV_2H_{0.6}$, as derived from the six-site model. The dashed line shows the behaviour of τ_l^{-1} estimated from the proton NMR measurements in $TaV_2H_{0.56}$ in the range 70–200 K [2].

3.4. Comparison with the NMR results

In this section we shall consider the NMR data for TaV_2H_x (TaV_2D_x) [1, 2] in more detail. We shall show, in particular, that some other unusual features of the NMR data can also be explained in terms of the microscopic picture of H motion following from our present QENS results.

The nuclear spin–lattice relaxation rates related to atomic motion, T_{1m}^{-1}, are described by sums of one or more terms, each of the general form [20]

$$T_{1m}^{-1} = \langle M^2 \rangle J(\omega_I, \omega_S, \tau_c). \tag{8}$$

Here $\langle M^2 \rangle$ is that part of the interaction of a nuclear spin with its environment that is caused to fluctuate by the motion, and $J(\omega_I, \omega_S, \tau_c)$ is the spectral density function of the fluctuations with the correlation time τ_c; ω_I and ω_S are the NMR frequencies of the resonant and non-resonant nuclei, respectively. Usually τ_c is approximately equal to the mean residence time of the hopping atom. $J(\omega_I, \omega_S, \tau_c)$ is known to have a maximum at the temperature at which the condition

$$\omega_I \tau_c \approx 1 \tag{9}$$

is fulfilled. The form of $J(\omega_I, \omega_S, \tau_c)$ depends on the model of the atomic motion. The temperature dependence of each of the measured ^1H, ^2D and ^{51}V spin–lattice relaxation rates in TaV_2H_x (TaV_2D_x) shows two peaks [1, 2]. In the region of the high-temperature maximum (290–360 K) the role of τ_c in equation (9) is played by τ_d, and in the region of the low-temperature maximum (50–180 K) this role is played by τ_l.

It is usually assumed that the temperature dependence of T_{1m}^{-1} in metal–hydrogen systems is determined only by changes in τ_c, i.e. the effective 'amplitude' $\langle M^2 \rangle$ of the fluctuations

is temperature independent. This assumption is well justified for the case of long-range diffusion. However, it may not be true for the localized H motion with the temperature-dependent fraction p of participating atoms. As it has been discussed in [21], for the case of $p \neq 1$ a single value of the observed relaxation rate may result from the fast transfer of spin polarization (*spin diffusion*), and the resulting value of T_{1m}^{-1} is expected to be proportional to p. Therefore the temperature dependence of p can contribute to changes in T_{1m}^{-1} via changes in $\langle M^2 \rangle$. Note that the width of a QENS line does not contain such a factor as $\langle M^2 \rangle$ depending on the 'amplitude' of the interaction of a nucleus with its environment. In this respect QENS data give more direct information on the parameters of the atomic motion, as compared to the spin-relaxation NMR data.

Figure 10 shows the temperature dependence of the hopping rate τ_l^{-1} resulting from the fit of the six-site model to our QENS data for $TaV_2H_{0.6}$. The dashed line in figure 10 shows the behaviour of τ_l^{-1}, as estimated from the proton NMR measurements for $TaV_2H_{0.56}$ in the range 70–200 K [2]. It should be noted that the proton NMR data were analysed in terms of the model of H hopping between a pair of sites [21]. For more complicated types of motion the relation between the NMR frequency and the value of τ_l^{-1} at the relaxation rate maximum is expected to differ from that of the two-site model. This may account for the difference between the absolute values of τ_l^{-1} found from the NMR and QENS data. Furthermore, the possibility of temperature-dependent p has not been allowed for in the analysis of the NMR data [2]. The effect of $p(T)$ on the values of τ_l^{-1} derived from the spin–lattice relaxation data is especially strong at low temperatures (much lower than the temperature of the low-T relaxation rate maximum). However, in the range 70–200 K the estimated effect of $p(T)$ on the temperature dependence of τ_l^{-1} does not exceed 20%.

We now consider the behaviour of the low-T maximum motional contribution to the proton spin–lattice relaxation rate, $(T_{1m}^{-1})_H^{LTmax}$, as a function of H concentration. The value of $(T_{1m}^{-1})_H^{LTmax}$ is found to increase strongly with increasing H content. For example, at the frequency of 64 MHz this value changes from 4.0 s^{-1} for $TaV_2H_{0.56}$ to 9.1 s^{-1} for $TaV_2H_{1.33}$ [2]. Such a behaviour is difficult to explain in terms of the usual approach. In fact, $(T_{1m}^{-1})_H$ for TaV_2H_x is mainly determined by ^1H–^{51}V dipole–dipole interaction [2] which is expected to give an x-independent contribution to the proton relaxation rate. It turns out, however, that the observed concentration dependence $(T_{1m}^{-1})_H^{LTmax}$ can be qualitatively described, if we take into account the temperature dependence of p. As the hydrogen content increases, the position of the low-T maximum of $(T_{1m}^{-1})_H$ shifts to higher temperatures. For example, at 64 MHz this maximum is observed at 90 K for $TaV_2H_{0.56}$ and at 167 K for $TaV_2H_{1.33}$ [2]. This shift reflects the decrease in τ_l^{-1} with increasing H content. Because of the strong temperature dependence of p (see figure 8), the value of p at the temperature of the low-T maximum of $(T_{1m}^{-1})_H$ in the concentrated hydride appears to be higher than in the dilute one. Since, as discussed above, $(T_{1m}^{-1})_H$ is expected to be proportional to p, the observed concentration dependence of $(T_{1m}^{-1})_H^{LTmax}$ can be attributed to changes in p at the temperature of the maximum. Indeed, the ratio of the values of $(T_{1m}^{-1})_H^{LTmax}$ for $TaV_2H_{1.33}$ and $TaV_2H_{0.56}$ at 64 MHz is about 2.27 [2], and the estimated ratio of p-values at the temperatures of the corresponding maxima (167 K and 90 K, respectively) is 1.8. The difference may be ascribed to the small ^1H–^1H dipolar contribution to $(T_{1m}^{-1})_H$ which is proportional to x.

The most intriguing feature of the NMR data for TaV_2H_x (TaV_2D_x) is the pronounced effect of isotope (H↔D) substitution on the ^{51}V spin–lattice relaxation rate $(T_{1m}^{-1})_V$ [1, 2]. The dominant contribution to $(T_{1m}^{-1})_V$ originates from the interaction between the electric quadrupole moment of ^{51}V and the fluctuating electric field gradient (EFG) produced by hopping H (D) atoms. Since only charge fluctuations are involved, for the same type of motion H and D atoms should give the same contribution to $(T_{1m}^{-1})_V$. As expected, the

observed amplitudes of the high-temperature maximum, $(T_{1m}^{-1})_V^{HTmax}$, related to τ_d^{-1}, are nearly the same for the hydrides and deuterides with the same x. However, the amplitude of the low-temperature maximum $(T_{1m}^{-1})_V^{LTmax}$ for the deuterides is nearly three times higher than for the hydrides with the same x [1, 2]. Thus the mean square amplitude of the EFG fluctuations (caused by the localized motion) at V sites in TaV_2D_x is considerably higher than in TaV_2H_x. This feature could not be described satisfactorily in terms of the approach [2] assuming $p = 1$. On the other hand, it may be qualitatively explained if we allow for the possibility of $p \neq 1$. The observed isotope effect suggests that for the same temperature the value of p for D atoms is higher than for H atoms because of the lower energy of excitation to a mobile state for deuterium.

3.5. Comparison with other Laves phase hydrides

It can be expected that for the other cubic Laves phase hydrides, where H atoms occupy only g sites, the microscopic picture of hydrogen motion is qualitatively the same as for TaV_2H_x. In fact, the existence of two frequency scales of H motion is consistent with the NMR data for $TiCr_2H_x$ [22], $ZrCr_2H_x$ [19], HfV_2H_x and ZrV_2H_x [23]. Recent QENS experiments on $ZrCr_2H_{0.45}$ [24] have confirmed the existence of a fast localized H motion similar to that found for TaV_2H_x. In all of these systems, at low x ($x \leqslant 2.5$), hydrogen atoms are known to occupy only g sites. However, the difference between the two frequency scales of H motion in these systems is not as high as in TaV_2H_x; therefore the additional low-temperature maximum of the spin–lattice relaxation rate is not observed for them. Instead, the localized H motion in these systems just contributes to changes in the low-temperature slope of the $T_1^{-1}(T)$ dependence.

Table 2. The positional parameters of H (D) atoms at g sites, the ratio of the metallic radii of elements A and B, the lattice parameters and the g–g distances r_1 and r_2 for the cubic Laves phase hydrides AB_2H_x. A typical uncertainty in the refined X- and Z-values is ±0.001. The values of a_0, r_1 and r_2 correspond to $x = 0.5$.

System	X	Z	Reference	R_A/R_B	a_0 (Å)	r_1 (Å)	r_2 (Å)
'Ideal'	0.063	0.875		1.225			
$ZrCr_2$–H ($ZrCr_2$–D)	0.063	0.872	[25]	1.250	7.28	1.11	1.27
ZrV_2–H (ZrV_2–D)	0.061	0.874	[26]	1.190	7.49	1.14	1.36
HfV_2–H (HfV_2–D)	0.061	0.872	[27]	1.174	7.42	1.13	1.35
TaV_2–H (TaV_2–D)	0.055	0.888	[6]	1.090	7.21	0.98	1.43

In order to find out why the difference between the two frequency scales of H motion is most pronounced for TaV_2H_x, we may compare the positional parameters of H atoms in different Laves phase hydrides. Table 2 shows the positional parameters X and Z of hydrogen at g sites of cubic Laves phase hydrides for which these parameters are known from the neutron diffraction measurements. It can be seen that for $ZrCr_2$–H ($ZrCr_2$–D), HfV_2–H (HfV_2–D) and ZrV_2–H (ZrV_2–D) the experimental values of X and Z are close to the corresponding 'ideal' ones. On the other hand, for TaV_2–H (TaV_2–D) there is a considerable difference between the experimental values of X and Z and the 'ideal' ones. This results in the H (D) displacements discussed in section 3.2. The actual positional parameters of H atoms can be rationalized in terms of the metallic radii R_A and R_B of the elements A and B forming the AB_2 intermetallic. It is known that for many intermetallic hydrides the hydrogen–metal distances are nearly the same as in the corresponding metal

hydrides [4, 13]. This means that for interstitial sites formed by different metal atoms (A_2B_2 in the case of g sites) one may expect displacements of hydrogen from the 'ideal' positions, if the ratio R_A/R_B deviates from its 'ideal' value (1.225 for Laves phase compounds). As can be seen from table 2, for TaV_2 the deviation of R_A/R_B from the 'ideal' value is the strongest. The value of R_A/R_B for TaV_2 appears to be one of the lowest among all Laves phase compounds [28]. Therefore we can conclude that the most pronounced separation of the g-site hexagons from each other in TaV_2H_x is related to the anomalously low R_A/R_B ratio.

Included in table 2 are also the lattice parameters a_0 and the g–g distances r_1 and r_2 calculated using the actual positional parameters of g sites. For all of the systems the values of a_0, r_1 and r_2 correspond to $x = 0.5$. It can be seen that for TaV_2H_x the distance r_1 is the shortest; this may account for the fastest localized H motion being found in this system. One may expect that the distance r_2 between the nearest g sites on different hexagons determines the long-range diffusivity. Indeed, the r_2-value for TaV_2H_x appears to be the longest, in spite of it having the lowest a_0. This correlates with the fact that the long-range H diffusion in TaV_2H_x is *slower* than in the other Laves phase hydrides [15]. On the other hand, for $ZrCr_2H_x$ having the shortest r_2 the long-range H diffusivity is found to be the highest among all Laves phase hydrides [18].

Thus, we can conclude that there is a clear correlation between the g–g distances r_1 and r_2 and the parameters of two types of H motion. The value of r_1 determines the rate of the localized H hopping, and the value of r_2 is related to the long-range H diffusivity. A decrease in r_1 and r_2 leads to an increase in the corresponding hopping rates. It should be noted, however, that this tendency is limited by the absorbing ability of compounds. Below a certain value of the lattice parameter a_0 the interstitial holes become too small to be occupied by hydrogen [13]. The a_0-values for TaV_2 and $ZrCr_2$ appear to be close to this limit; therefore these compounds have both short distances r_1 or r_2 and reasonable hydrogen absorption properties.

4. Conclusions

The analysis of our quasielastic neutron scattering data for C15-type TaV_2H_x has shown that the diffusive motion of hydrogen in this system can be described in terms of two jump processes with different frequency scales. The faster process implies H jumps within the hexagons formed by g sites; this localized motion is characterized by the hopping rate τ_l^{-1}. The slower process with the hopping rate τ_d^{-1} corresponds to jumps from one g-site hexagon to the other. The value of τ_l^{-1} strongly depends on hydrogen concentration, decreasing with increasing H content. It is found that only a fraction p of H atoms participates in the fast localized motion, and this fraction increases with temperature. The fraction $1-p$ of 'static' H atoms (with the hopping rates much lower than τ_l^{-1}) is likely to originate from the H–H interaction leading to the formation of some ordered atomic configurations at low temperatures. Thus the tendency towards long-range hydrogen ordering at higher x [6] is expected to suppress the fast localized H motion.

The model of H motion following from our QENS results suggests plausible explanations of a number of puzzling features of previous experiments, including high values of the apparent jump lengths in Laves phase hydrides [16–18], the strong x-dependence of the amplitude of the low-T peak of the proton spin–lattice relaxation rate [2] and the unusual effect of H $\leftrightarrow$ D substitution on the ^{51}V spin–lattice relaxation in TaV_2H_x (TaV_2D_x) [1, 2]. Comparison of the structural parameters of Laves phase hydrides with g-site occupation

and the corresponding hydrogen mobilities shows that the parameters of H motion strongly depend on the g–g distances r_1 (within the hexagons) and r_2 (between different hexagons). For TaV_2H_x the r_2/r_1 ratio is the highest among the Laves phase hydrides for which the hydrogen diffusion has been studied. Therefore the difference between the frequency scales τ_l^{-1} and τ_d^{-1} is most pronounced for TaV_2H_x.

Acknowledgments

This work was partially supported by the Russian Foundation for Fundamental Research (grant 96-02-16517). AVS acknowledges the financial support of the Alexander von Humboldt Foundation and the Universität des Saarlandes.

References

[1] Skripov A V, Belyaev M Yu, Rychkova S V and Stepanov A P 1989 *J. Phys.: Condens. Matter* **1** 2121
[2] Skripov A V, Rychkova S V, Belyaev M Yu and Stepanov A P 1990 *J. Phys.: Condens. Matter* **2** 7195
[3] Lynch J F 1981 *J. Phys. Chem. Solids* **42** 411
[4] Somenkov V A and Irodova A V 1984 *J. Less-Common Met.* **101** 481
Somenkov V A and Irodova A V 1984 private communication
[5] Stonadge P R 1992 *PhD Thesis* University of Birmingham
[6] Fischer P, Fauth F, Skripov A V, Podlesnyak A A, Padurets L N, Shilov A L and Ouladdiaf B 1997 *J. Alloys Compounds* **253+254** 282
[7] Berk N F, Rush J J, Udovic T J and Anderson I S 1991 *J. Less-Common Met.* **172–174** 496
[8] Skripov A V, Cook J C, Karmonik C and Hempelmann R 1996 *J. Phys.: Condens. Matter* **8** L319
[9] Bée M 1988 *Quasielastic Neutron Scattering* (Bristol: Hilger)
[10] Yvon K 1984 *J. Less-Common Met.* **103** 53
[11] Schönfeld C, Hempelmann R, Richter D, Springer T, Dianoux A J, Rush J J, Udovic T J and Bennington S M 1994 *Phys. Rev.* B **50** 853
[12] Phillips W A 1987 *Rep. Prog. Phys.* **50** 1657
[13] Yvon K and Fischer P 1988 *Hydrogen in Intermetallic Compounds I* ed L Schlapbach (Berlin: Springer) p 87
[14] Chudley C T and Elliott R J 1961 *Proc. Phys. Soc.* **77** 353
[15] Majer G, Renz W, Seeger A, Barnes R G, Shinar J and Skripov A V 1995 *J. Alloys Compounds* **231** 220
[16] Schönfeld C 1992 *PhD Thesis* Technische Hochschule Aachen
[17] Havill R L, Titman J M, Wright M S and Crouch M A 1989 *Z. Phys. Chem., NF* **164** 1083
[18] Renz W, Majer G, Skripov A V and Seeger A 1994 *J. Phys.: Condens. Matter* **6** 6367
[19] Skripov A V and Belyaev M Yu 1993 *J. Phys.: Condens. Matter* **5** 4767
[20] Barnes R G 1997 *Hydrogen in Metals III* ed H Wipf (Berlin: Springer) p 93
[21] Lichty L R, Han J W, Ibanez-Meier R, Torgeson D R, Barnes R G, Seymour E F W and Sholl C A 1989 *Phys. Rev.* B **39** 2012
[22] Bowman R C, Craft B D, Attalla A and Johnson J R 1983 *Int. J. Hydrogen Energy* **8** 801
[23] Skripov A V, Belyaev M Yu, Rychkova S V and Stepanov A P 1991 *J. Phys.: Condens. Matter* **3** 6277
[24] Skripov A V, Pionke M, Randl O and Hempelmann R 1998 to be published
[25] Irodova A V, Lavrova O A, Laskova G V and Padurets L N 1982 *Sov. Phys.–Solid State* **24** 22
[26] Didisheim J J, Yvon K, Shaltiel D, Fischer P, Bujard P and Walker E 1979 *Solid State Commun.* **32** 1087
[27] Irodova A V, Glazkov V P, Somenkov V A and Shil'shtein S Sh 1980 *Sov. Phys.–Solid State* **22** 45
[28] Nevitt M V 1963 *Electronic Structure and Alloy Chemistry of the Transition Elements* ed P A Beck (New York: Interscience)